Scientific Research Publishing

Journal of Modern Physics, 2022, 13, 285-300
https://www.scirp.org/journal/jmp
ISSN Online: 2153-120X
ISSN Print: 2153-1196

Non Ideal Schottky Barrier Diode's Parameters Extraction and Materials Identification from Dark *I-V-T* Characteristics

M. Bashahu, D. Ngendabanyikwa, P. Nyandwi

Department of Physics and Technology, Institute of Applied Pedagogy, Bujumbura, Burundi
Email: bashahuma@yahoo.fr

How to cite this paper: Bashahu, M., Ngendabanyikwa, D. and Nyandwi, P. (2022) Non Ideal Schottky Barrier Diode's Parameters Extraction and Materials Identification from Dark *I-V-T* Characteristics. *Journal of Modern Physics*, **13**, 285-300.
https://doi.org/10.4236/jmp.2022.133020

Received: December 8, 2021
Accepted: March 6, 2022
Published: March 9, 2022

Abstract

Several parameters of a commercial Si-based Schottky barrier diode (SBD) with unknown metal material and semiconductor-type have been investigated in this work from dark forward and reverse *I-V* characteristics in the temperature (*T*) range of [274.5 K - 366.5 K]. Those parameters include the reverse saturation current (I_s), the ideality factor (n), the series and the shunt resistances (R_s and R_{sh}), the effective and the zero bias barrier heights (Φ_B and Φ_{B0}), the product of the electrical active area (A) and the effective Richardson constant (A^{**}), the built-in potential (V_{bi}), together with the semiconductor doping concentration (N_A or N_D). Some of them have been extracted by using two or three different methods. The main features of each approach have been clearly stated. From one parameter to another, results have been discussed in terms of structure performance, comparison on one another when extracted from different methods, accordance or discordance with data from other works, and parameter's temperature or voltage dependence. A comparison of results on Φ_B, Φ_{B0}, n and N_A or N_D parameters with some available data in literature for the same parameters, has especially led to clear propositions on the identity of the analyzed SBD's metal and semiconductor-type.

Keywords

SBD, Dark Forward and Reverse *I-V-T* Characteristics, Different Parameters Extraction Methods, Identification of the Structure's Metal and Semiconductor-Type

1. Introduction

Rectifying metal-semiconductor (MS) contacts, also known as Schottky barrier diodes (SBDs), have received an increasing attention due to their applications in

photovoltaic solar cells [1] [2] [3] [4], field effect transistors (FETs) [5], infrared high-speed detectors, electronic switching and other high-frequency devices [6] [7] [8] [9]. Many reports on SBDs physical properties have been proposed in order to better understand the performance of those structures and related devices. The four SBD's key parameters are the reverse saturation current (I_s), the ideality factor (n), the series resistance (R_s) and the effective Schottky barrier height (SBH, Φ_B) [10]. Together with the SBH at zero bias (or the asymptotic SBH) (Φ_{B0}), the electrical active area (A), the effective Richardson constant (A^{**}) and the semiconductor doping concentration (N_A or N_D), those parameters can be extracted by using different methods based on current-voltage (I-V) characteristics [11]-[28]. Besides this first group of methods, capacitance-voltage (C-V) techniques are used to extract majority carrier concentration (N_A or N_D), activation energy (E_A), densities (n_{is}) and energy levels (E_{is}) of interface states. In addition, photo-response measurements, which involve various spectroscopic techniques, are implemented in order to extract parameters such as band-gap, impurity and doping concentration, layer thickness, surface roughness and texture [29] [30]. Methods from those three groups are combined in some reports [4] [31]-[37].

While several methods from those groups are analytical ones, numerical techniques are also used [1] [2] [9] [38] [39] [40] [41] [42]. Moreover, as shown in some review reports [43] [44] [45] [46], from one method to another, two or several parameters can be simultaneously extracted; dc or ac, static or dynamic, fixed or varying frequency and temperature operation's conditions can be applied; different current transport mechanisms may be taken into account; results can be temperature or voltage dependent; and they may be compared one another when different methods are combined.

The SBD analyzed in this work is a commercial Si-based one from ST Microelectronics, for which neither the metal nor the semiconductor-type (p- or n-) were specified in the relevant catalog. By using dark forward and reverse current-voltage (I-V) characteristics at different temperatures, together with different approaches, our objective was three-fold: firstly to extract different parameters of that structure, secondly to discuss our results, and thirdly to especially come to identify the SBD's metal and semiconductor-type.

2. Experimental Details

The SBD sample of this analysis is shown magnified in **Figure 1** and has the following actual specifications: blue color, BAT 48 as trade mark, diameter and length of the central part equal to 0.15 cm and 0.3 cm, respectively, diameter and length of each of the two terminal's wires equal to 0.7 mm and 3.0 cm, respectively.

Reverse and forward I-V-T characteristics of the diode were measured in dark conditions over bias voltage and temperature ranges of [−2.5; +0.5] V and [274.5; 336.5] K, respectively. A common experimental arrangement of simple equipments

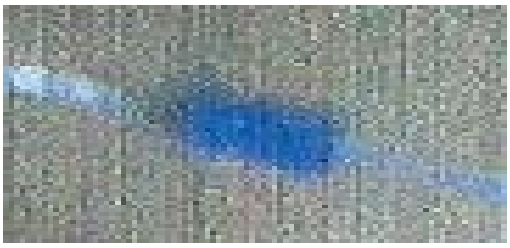

Figure 1. Magnified view of the SBD of this study.

has been used for that purpose. These include notably a power supply with d.c emf fixed to a maximum value E_0 = 2.5 V; a rheostat mounted with the power supply in such a way to vary the emf, an ammeter and a voltmeter for *I-V* measurements; an ice bath and an electrical heater to change thermal conditions of the sample, and a thermometer for temperature measurements.

3. Extracted Parameters, Used Methods, Results and Discussion

3.1. R_{sh} from Reverse *I-V* Plots

The complete representation of a real diode's *I-V* characteristic is given by Equation (1) [47]:

$$I = I_s\left\{\exp\left[\frac{q(V-R_sI)}{nK_BT}\right]-1\right\}+\frac{V-R_sI}{R_{sh}} \quad (1)$$

where I_s, n, R_s and R_{sh} are the diode's reverse saturation current, ideality factor, series resistance and shunt resistance, respectively, while q is the absolute value of the electronic charge and K_B is the Boltzmann's constant. The first term of the sum in Equation (1) represents the diode current and the second term describes the current through the shunt resistance (I_p). The simplest way to extract R_{sh} or the related shunt conductance (G_p) consists in determining the slope of the straight line representing the reverse *I-V* characteristic. That slope is given by Equation (2) [48]:

$$G_p = \frac{1}{R_{sh}} = \frac{\Delta I_p}{\Delta V} \quad (2)$$

For the considered temperature range, the obtained SBD's reverse *I-V* lines (**Figure 2** is the plot of such a line at T = 286.5 K) were so merged that they have led to an almost constant shunt resistance: $R_{sh} = (4.93 \pm 0.07) \times 10^4\ \Omega$. This has been a proof of the scarcity of crystal irregularities or defects in the bulk and at the edges of our SBD, through which current losses could occur.

3.2. I_s, R_s and n from Forward lnI_d-V Plots

With the assumption of thermoionic emission (TE) as the prevailing charge transport mechanism in the SBD, the forward diode's *I-V* characteristic is given by [19] [47] [49]

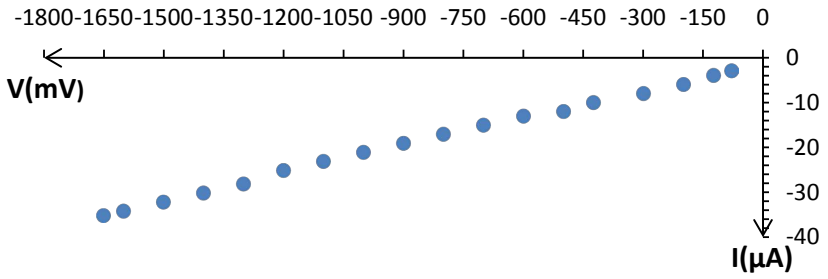

Figure 2. Plot of reverse *I-V* data for the SBD at 286.5 K.

$$I_d = I_s\left[\exp\left(\frac{qV}{nK_BT}\right)-1\right] \tag{3}$$

In Equation (3), the reverse saturation current (I_s) is expressed as

$$I_s = AA^{**}\left(\frac{-\Phi_B}{K_BT}\right) \tag{4}$$

where T is the diode's absolute temperature, A is the junction's electrically active area, A^{**} is the effective Richardson constant and Φ_B is the effective Schottky barrier height (SBH). When the forward bias $V > \frac{3K_BT}{q}$, Equation (3) is given by [50]

$$I_d = I_s\exp\left(\frac{qV}{nK_BT}\right) \tag{5}$$

According to Equation (5), n and I_s parameters can be, respectively, extracted from the slope and the intercept of the linear region (diffusion line) in the plot of the experimental $\ln I_d$- V data. Nevertheless, the presence of a parasitic series resistance affects the I-V characteristic mostly at high voltages. To account for this, Equation (5) is re-arranged to become

$$I_d = I_s\exp\left[\frac{q(V-R_sI)}{nK_BT}\right] \tag{6}$$

Using Equation (6) and following the Cowley and Sze method (ref. no. 2 in [43]), one extracts R_s from the gap ΔV (on the V-axis) between the actual $\ln I_d$ vs V curve and the diffusion line. **Figure 3** is the plot of that curve for our SBD at one fixed temperature. On that plot, as different R_s are obtained at different I_d in the related region, a mean R_s-value is extracted.

Values of n, I_s and R_s determined according to the previous methodology are summarized in **Figure 4**.

$n(T)$ data from **Figure 4** exhibit a somehow wavy trend, while results from other works state a slight decrease of the ideality factor with increasing temperature [19] [22] [36] [51]. Nevertheless, values of n for our SBD are higher than those commonly observed for c-Si solar cells [44]. Moreover, the ideality factor of our sample has values in good agreement with those of other investigated Si-based SBDs, e.g.: $1.2 < n < 2.7$ for Pt/p-Si [16].

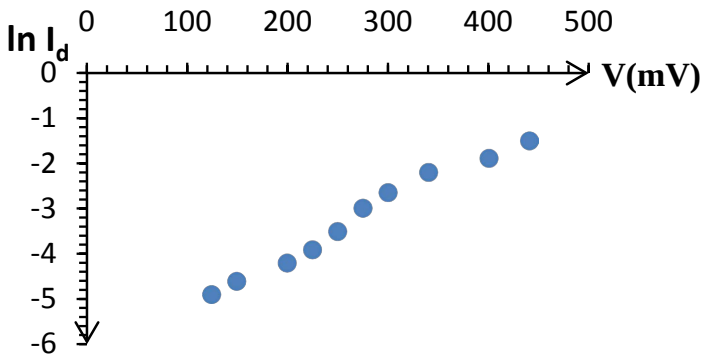

Figure 3. Plot of $\ln I_d$- V data for the SBD of this study at $T = 317$ K.

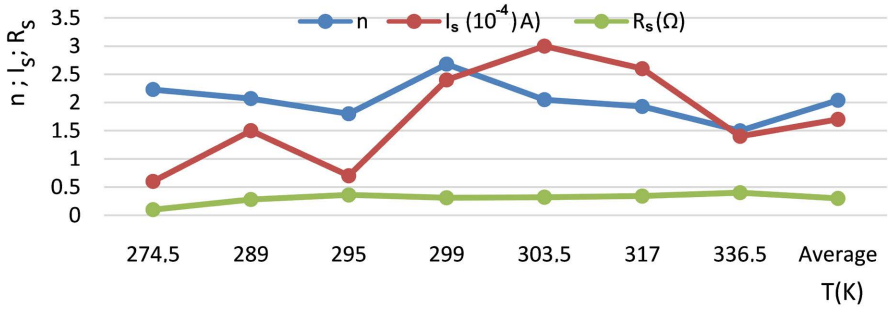

Figure 4. Plots of n, I_s and R_s vs T data for the SBD of this study.

The average series resistance (R_s) of our SBD is much higher than R_s-values commonly observed for c-Si solar cells [43]. This is likely due to high resistivity (ρ) of Si-based SBDs (e.g.: ρ is equal to 15 Ω cm for Tb/p-Si; 8 Ω cm for Ru/n-Si and 1 Ω cm for Pt/n-Si) [52], compared to resistivity of p-Si and n-Si materials (and thus of p-n Si junctions). As examples, ρ lies in the ranges $[4 \times 10^{-4}; 3 \times 10^{-2}]$ Ω cm and $[10^{-4}; 6 \times 10^{-2}]$ Ω cm for n-Si and p-Si, respectively, when the doping concentration decreases from 10^{+21} cm^{-3} to 10^{+18} cm^{-3} [6].

At its side, the reverse saturation current (I_s) may increase with increasing temperature according to Equation (4). That theoretical trend is not well evidenced by results of **Figure 4**. Nevertheless, those results do not depart too much from I_s-values observed elsewhere for some Si-based SBDs in the same temperature and voltage ranges. As examples, I_s is equal to 7×10^{-5} A for a Cr Si_2/n-Si junction at 300 K and for $V \in [0.12; 0.35]$ V [53], and to 4×10^{-4} A for an epitaxial $CoSi_2$/n-Si diode with an area of 0.61 mm^2, at 292 K and $V \in [0.2; 0.5]$ V [51].

3.3. Φ_B and AA^{**} from the Activation Energy Method

From Equations (4) and (5), assuming $n \approx 1$, the SBD's forward I-V characteristic is expressed as

$$I = AA^{**}T^2 \exp\left[-\left(\frac{\Phi_B - qV}{K_B T}\right)\right] \tag{7}$$

and thus

$$\ln\left(I/T^2\right)=\ln\left(AA^{**}\right)-\left(\frac{\Phi_B-qV}{K_B}\right)\frac{1}{T} \tag{8}$$

The activation energy method is based on the plot of experimental $\ln(I/T^2)$-$(1/T)$ data at a given voltage bias $V>\frac{3K_BT}{q}$. From such an Arrhenius (or Richardson) plot, the effective Schottky barrier height (Φ_B) and the AA^{**} product (of the contact's electrically active area and the effective Richardson constant) can be derived from the negative slope and the intercept of the expected resulting straight line, respectively. Based on experimental forward I-V-T data on the SBD of this analysis, results of such a determination are shown in Figure 5.

The SBHs in Figure 5 are estimates of actual Φ_B since too many approximations are used in the present method. Moreover, experimental data points have been found scattered in each $\ln(I/T^2)$-$(1/T)$ plot. Nevertheless, a clear increase of the SBH with increasing bias voltage is noticed in agreement with theory (e.g. in Section 3.4).

The AA^{**} mean product is equal to 2.35×10^{-6} A/K^2. Using that result and the effective Richardson constants of 12 and 32×10^4 A·m^{-2}·K^{-2} for n-Si and p-Si, respectively [6] [52], one finds the contact's electrically active area A of the SBD equal to 2.23 μm^2 and 7.81 μm^2 for n-Si and p-Si, respectively. Those values correspond to diameters of 1.69 μm and 3.15 μm, respectively, which are clearly lower than the measured diameter (=0.7 mm) of each terminal's wire.

3.4. Φ_{B0} from the SBH's Bias Dependence Behavior

The basic equation used to estimate the SBH within the TE theory is obtained by combining Equations (3) and (4):

$$I_d=AA^{**}T^2\exp\left(\frac{-\Phi_B}{K_BT}\right)\left[\exp\left(\frac{qV}{K_BT}\right)-1\right] \tag{9}$$

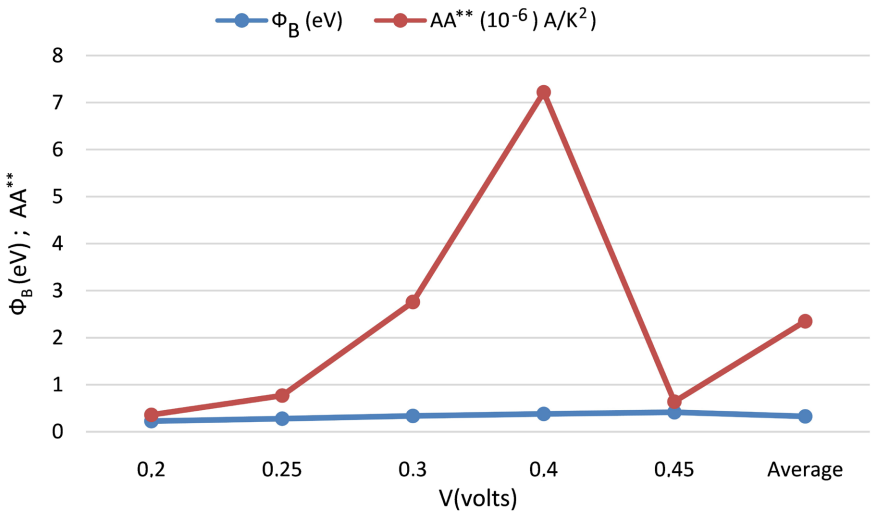

Figure 5. Results of Φ_B and AA^{**} obtained from Richardson's plots.

As the SBH is strongly dependent on the electrical field in the depletion region and thus on the applied bias, Φ_B is commonly expressed as [16] [19]

$$\Phi_B = \Phi_{B0} + \beta V \tag{10}$$

where Φ_{B0} is the barrier height at zero bias (or the asymptotic barrier height) and β is assumed to be a positive constant over the region of measurement. That means an increase of the SBH with increasing bias voltage. This trend is experimentally observed from results in **Figure 5**. If the ideality factor in defined as in Equation (11)

$$\frac{1}{n} = 1 - \beta \tag{11}$$

then the forward *I*-*V* characteristic of Equation (9) becomes:

$$I_d = I_0 \exp\left(\frac{qV}{nK_BT}\right)\left[1 - \exp\left(\frac{-qV}{K_BT}\right)\right] \tag{12}$$

where

$$I_d = AA^{**}T^2 \exp\left(\frac{-\Phi_{B0}}{K_BT}\right) \tag{13}$$

For bias voltage $V > \frac{3K_BT}{q}$, Equation (12) reduces in the following simple form

$$I_d \approx I_0 \exp\left(\frac{qV}{nK_BT}\right) \tag{14}$$

From Equation (13), the SBH at zero bias is expressed as:

$$\Phi_{B0} = K_BT \ln\left(AA^{**}T^2/I_0\right) \tag{15}$$

where I_0 is the reverse saturation current extrapolated at zero bias. Equation (15) offers a way to determine Φ_{B0} using AA^{**} data from **Figure 5** and I_s-values from **Figure 4** ($I_0 \approx I_s$ since extrapolated at zero bias). The results of such a determination are shown in **Figure 6**.

In accordance with Equation (10), values of Φ_{B0} are lower than those of Φ_B from **Figure 5**. Nevertheless, Φ_{B0}-T data exhibit a wavy trend whereas results from other works state that the SBH and its value at zero bias slightly increase with increasing temperature [19] [54].

3.5. *n*, R_s and Φ_B from the Auxiliary Cheung's Functions

In this method, firstly Equation (6) (with $I_d = I$) is re-arranged as

$$\ln I = \ln I_s + \frac{qV}{nK_BT} - \frac{qR_sI}{nK_BT} \tag{16}$$

and thus

$$V = \frac{nK_BT}{q}\ln I + R_sI - \frac{nK_BT}{q}\ln I_s \tag{17}$$

Differentiating Equation (17) provides:

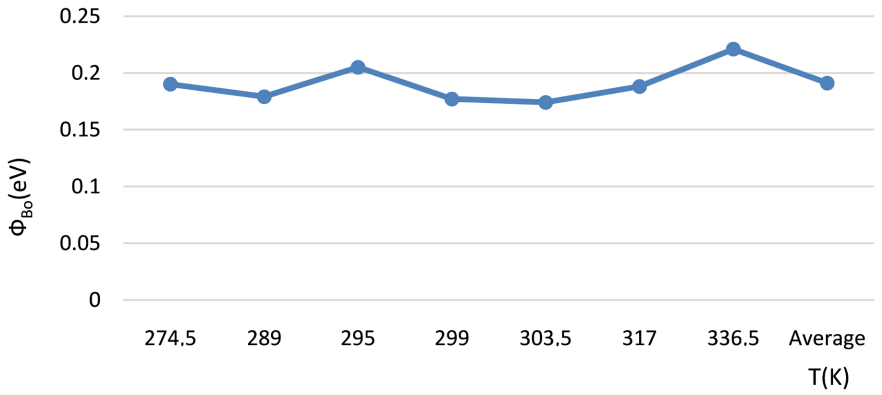

Figure 6. Results of Φ_{B0} vs T data for the SBD of this study.

$$\mathrm{d}V = \frac{nK_BT}{q}\mathrm{d}\left(\ln I\right) + R_s\mathrm{d}I \tag{18}$$

and thus

$$\frac{\mathrm{d}V}{\mathrm{d}\left(\ln I\right)} = \frac{nK_BT}{q}R_sI \tag{19}$$

Equation (19) shows that, from experimental forward I-V data at a given temperature, the curve $\left[\mathrm{d}V/\mathrm{d}\left(\ln I\right)\right]$-$I$ is a straight line from which R_s and nK_BT/q can be extracted as the slope and the intercept, respectively.

Secondly, combining Equations (4) and (6) (with $I_d = I$) yields

$$\ln\left(\frac{I}{AA^{**}T^2}\right) + \frac{\Phi_B}{K_BT} = \frac{q}{K_BnT}V - \frac{q}{K_BnT}R_sI \tag{20}$$

Equation (20) is re-arranged to become

$$H\left(I\right) = R_sI + n\Phi_B \tag{21}$$

where

$$H\left(I\right) = V - \frac{nK_BT}{q}\ln\left(\frac{I}{AA^{**}T^2}\right) \tag{22}$$

Equations (19), (21) and (22) are the three auxiliary Cheung's functions [14]. Using the AA^{**} mean value of Figure 5 and experimental forward I-V data at a given temperature, allows one to get $H(I)$ data from Equation (22). The plot of those $H(I)$ data (Equation (21)) leads to a straight line from which R_s and $n\Phi_B$ can be extracted as the slope and the intercept, respectively. Figure 7 shows a curve of $[\mathrm{d}V/\mathrm{d}(\ln I)]$-$I$ data at a fixed temperature. Its points are quite scattered, whereas $H(I)$ data present a good linear behaviour at bias voltages $V > \frac{3K_BT}{q}$ as illustrated in Figure 8.

The values of n, R_s and Φ_B derived by using the previous procedure are presented in Figure 9.

It is shown that values of the ideality factor obtained from $[\mathrm{d}V/\mathrm{d}(\ln I)]$-$I$ plots (average n = 1.65) are quite lower than those extracted from $\ln I_d$-V plots (in

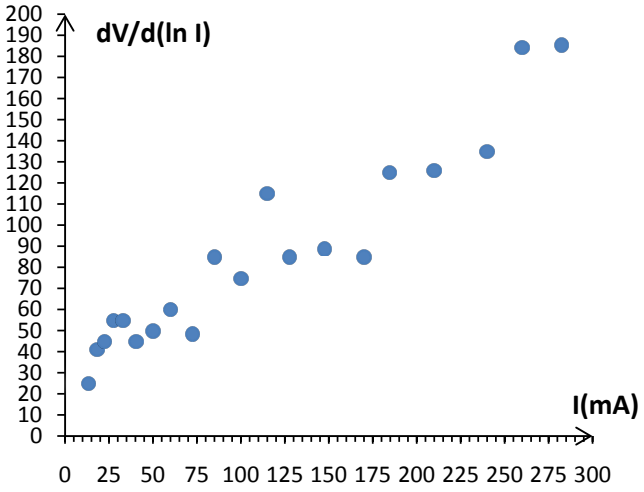

Figure 7. Plot of [d V/d(ln$I$)]-I data for the SBD of this study at T = 295 K.

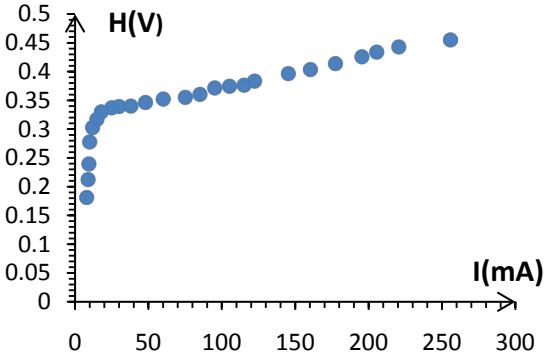

Figure 8. Plot of $H(I)$ data for the SBD of this analysis at T = 299.5 K.

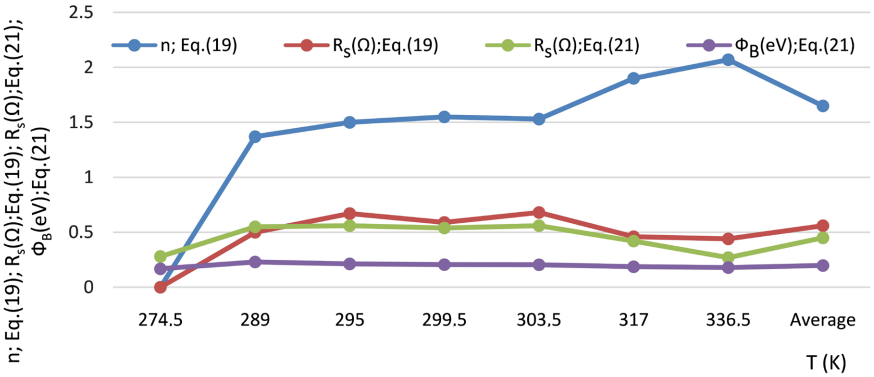

Figure 9. Results of n, R_s and Φ_B extracted from the auxiliary Cheung's functions.

Figure 4, average n = 2.04). Moreover, while $n(T)$ data from Figure 4 show a wavy trend, $n(T)$ results of the present method ([d V/d(lnI)]-I plots) seem to increase with increasing temperature.

A comparison of R_s-results of Figure 4 and Figure 5 shows that [d V/d(lnI)]-I plots yield higher values (mean R_s = 0.56 Ω), followed by data from H-I plots (mean R_S = 0.45 Ω), lnI_d-V plots leading to lower results (mean R_s = 0.30 Ω).

The auxiliary Cheung's functions method leads also to lower SBHs (mean Φ_B = 0.198 eV) than the activation energy method (in **Figure 5**, mean Φ_B = 0.325 eV). Moreover, a mean trend of SBH data from the Cheung's method is a decrease with increasing temperature and with increasing ideality factor. This is in accordance with statements from other works [14] [16] [49] [51].

3.6. V_{bi} from the Maximum Forward Current Method

At a given temperature, the SBD's maximum forward current ($I_d = I_{\max}$) is recorded at bias voltage V equal to the junction's built-in potential (V_{bi}), for which Equation (14) becomes [19]

$$I_{\max} \approx I_0 \exp\left(\frac{qV_{bi}}{nK_BT}\right) \tag{23}$$

or

$$\ln I_{\max} \approx \ln I_0 + \frac{qV_{bi}}{nK_B}\frac{1}{T} \tag{24}$$

Therefore, in the experimental I-V characteristics at different temperatures, accounting only for data corresponding to $I_{\max}$, one gets a plot of $\ln I_{\max}$-$\frac{1}{T}$. On the expected resulting straight line, the V_{bi} and $I_0 \approx I_s$ parameters are extracted from the slope and intercept, respectively. Estimates obtained by using that procedure and n-values of **Figure 9**, for the SBD and temperature range of this analysis, have been: V_{bi} = 0.496 V and $I_s = 0.34 \times 10^{-4}$ A, respectively.

3.7. N_A or N_D from Reverse I-V-T Data

In forward bias conditions, the SBH increases with increasing bias voltage as shown in **Figure 5** (Section 3.3) and Section 3.4. At the opposite, in reverse bias case, the main effect is the lowering of the SBH with the applied bias voltage $|V|$. In that case, the reverse current is expressed as [19]

$$I_R = I_0 \exp\left[\frac{q}{K_BT}\left(\frac{qE}{4\pi\varepsilon_s}\right)^{1/2}\right] \tag{25}$$

where I_0 is the reverse current at zero bias and the E quantity is given by

$$E = \left[\frac{2qN}{\varepsilon_s}\left(|V| + V_{bi} - \frac{K_BT}{q}\right)\right]^{1/2} \tag{26}$$

with ε_s the semiconductor's dielectric constant. If $V_{eff} = |V| + V_{bi} \gg \frac{K_BT}{q}$, then Equation (25) becomes

$$I_R \approx I_0 \exp\left(\alpha V_{eff}^{1/4}\right) \tag{27}$$

where the α parameter is expressed as

$$\alpha = \frac{q}{K_BT}\left(\frac{q}{4\pi\varepsilon_s}\right)^{1/2}\left(\frac{2qN}{\varepsilon_s}\right)^{1/4} \tag{28}$$

Equation (27) may be also written as

$$\ln I_R \approx \ln I_0 + \alpha V_{eff}^{1/4} \tag{29}$$

According to Equation (29), by using experimental reverse I-V data at a given temperature, together with the V_{bi} -value stated in section 3.6, $\varepsilon_s = 11.9\varepsilon_0$ for Si [19], and $\varepsilon_0 = 8.854\times10^{-12}\ \mathrm{F\cdot m^{-1}}$ [55], one gets a plot of $\ln I_R$-$V_{eff}^{1/4}$ data, which is expected to yield a straight line, and of which $I_0 \approx I_s$ and α (thus $N = N_A$ or N_D) parameters can be extracted from the intercept and the slope, respectively. An example of such a plot is shown in **Figure 10**. The N and $I_0 \approx I_s$ results obtained by following that procedure are given in **Figure 11**.

A comparison of our SBD reverse saturation current's results shows that the reverse I-V-T data method leads to slightly lower values (**Figure 11**, mean I_s = 1.31×10^{-4} A) than those from the forward.

lnI_d-V plots (**Figure 4**, mean I_s = 1.7×10^{-4} A). Moreover, the reverse I-V-T data method appears to be better than the lnI_d-V one for I_s-parameter extraction, since its results clearly exhibit an increase of reverse saturation current with increasing temperature, in accordance with theory.

Furthermore, for the SBD and the temperature range of this analysis, the semiconductor (Si)'s average doping concentration is found equal to 6.06×10^{18}

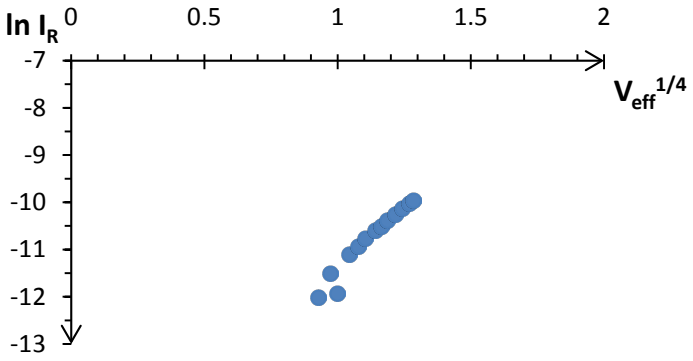

Figure 10. Plot of $\ln I_R$ vs $V_{eff}^{1/4}$ data points for the SBD of this study at T = 299.

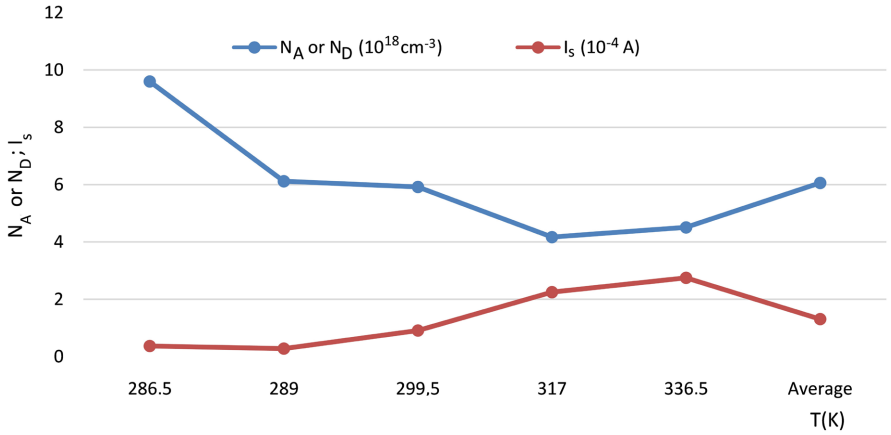

Figure 11. Results of N_A or N_D and I_s obtained from reverse I-V-T data.

Table 1. Synthesis of the obtained results and the used methods for SBD's parameters extraction in this analysis.

N°	Parameter	mean value	Extraction method	Comments
1	R_{sh}	$(4.93 \pm 0.07) \times 10^4\ \Omega$	Slope of reverse I-V plots	Not temperature dependent
2	n	2.04	$\ln I_d$- V plots	Temperature (T) dependent
		1.65	$[\mathrm{d}V/\mathrm{d}(\ln I)]$-$I$ plots	Increases with increasing T
3	R_s	0.30 Ω	$\ln I_d$- V plots	Increases with increasing T
		0.56 Ω	$[\mathrm{d}V/\mathrm{d}(\ln I)]$-$I$ plots	Temperature dependent
		0.45 Ω	Cheung's H-I plots	Temperature dependent
4	I_s	1.7×10^{-4} A	$\ln I_d$- V Plots	Increases with increasing T
		0.34×10^{-4} A	$I_{\max}$-$(1/T)$ plots	----
5	Φ_B	0.325 eV	Arrhenius plots	Increases with increasing V
		0.198 eV	Cheung's H-I plots	Decrease with increasing T
6	AA^{**}	2.35×10^{-6} A·K^{-2}	Arrhenius plots	Increases with increasing V
7	Φ_{B0}	0.191 V	V dependence of Φ_B	Temperature dependent
8	V_{bi}	0.496 V	$I_{\max}$-$(1/T)$ plots	----
9	N_A or N_D	$6.06 \times 10^{+18}$ cm^{-3}	Reverse I-V-T data	Decreases with increasing T

cm^{-3}. This indicates that, either n- or p-type, the actual Si material has a resistivity ρ of about 10^{-2} Ω cm [6].

3.8. Results Summary

For the SBD and the temperature range of this analysis, Table 1 shows in synthesis the obtained parameters' mean values and the extraction methods implemented so far.

3.9. Device Materials Identification

On one hand, the following data on some SBDs are reported amongst others in literature: 1) $\Phi_B = (0.272 \pm 0.005)$ eV and $\Phi_{B0} = (0.196 \pm 0.008)$ eV for a typical PtSi/p-Si structure, whereas $\Phi_B \in [0.847; 0.868]$eV for a Pt Si/n-Si diode at room temperature [16]; 2) $\Phi_B = 0.25$ eV for an Au/p-Si (chem.) contact, and $\Phi_B = 0.20$ eV for a PtSi/p-Si (back sputtering) diode from I-V data [6]; 3) $n \in [1.2; 2.7]$ for Pt/p-Si [16]; 4) with a doping concentration of 10^{+18} cm^{-3}, the resistivity, $\rho = 3 \times 10^{-2}$ Ω cm and 6×10^{-2} Ω cm for n-Si and p-Si materials, respectively [6]. On the other hand, the parameters' results obtained for the SBD and the temperature range of this study are presented in Table 1. A comparison of results on the same parameters in those two sets of data, allows one to certify that the SBD of this analysis is either Pt Si/p-Si or Au/p-Si.

4. Conclusion

As shown in the synthesis of Table 1, from I-V-T measurements and the use of different methods, up to nine parameters have been extracted on a Si-based MS

contact with unknown metal and semiconductor-type materials. Two of those parameters, *i.e.* the shunt resistance (R_{sh}) and the semiconductor doping concentration (N_A or N_D), have been derived from reverse *I-V-T* data. All the remaining seven parameters have been determined from forward *I-V-T* data. Those are the ideality factor (n), the series resistance (R_s), the reverse saturation current (I_s), the effective Schottky barrier height (SBH, Φ_B), the SBH at zero bias (Φ_{B0}), the product of the contact's electrical active area (A) and the effective Richardson constant (A^{**}), and the built-in potential (V_{bi}). Some of those seven parameters have been extracted by using two or three different approaches. The main features of each approach, including prevailing current transport mechanism, operation conditions and other assumptions, have been clearly stated. From one parameter to another, results have been discussed in terms of structure performance, parameter's temperature or voltage bias dependence, accordance or discordance with data from other works, and comparison on one another of results obtained from different methods. Furthermore, a comparison of results on the n, Φ_B, Φ_{B0}, and N_A or N_D parameters of Table 1 with some available data on the same parameters in literature, has led to state that the analyzed SBD is either Pt Si/p-Si or Au/p-Si.

Conflicts of Interest

The authors declare no conflicts of interest regarding the publication of this paper.

References

[1] Sellai, A. and Ouennoughi, Z. (2005) *International Journal of Modern Physics C*, **16**, 1043-1050. https://doi.org/10.1142/S0129183105007704

[2] Ku, J., Min, Y., Kim, J., *et al.* (2005) GAAS: Novel SPICE Macro Modeling for an Integrated Si Schottky Barrier Diode. 13*th GAAS Symposium*, Paris, 3-4 October 2005, 409-412.

[3] Tan, Z., Hong, L., Liu, J.-M., *et al.* (2019) *NPG Asia Materials*, **11**, Article No. 20. https://doi.org/10.1038/s41427-019-0120-3

[4] Allen, N.P. (2014) Electrical Characterization of Ruthenium Dioxide Schottky Contacts on Ga N. Thesis (for Master of Sciences in Electrical Engineering), Virginia Polytechnic Institute and State University, Blacksburg.

[5] Pearman, D. (2007) Electrical Characterization and Modeling of Schottky Barrier Metal Source/Drain MOSFETS. PhD Thesis, The University of Warwick, Coventry.

[6] Sze, S.M. (1969) Physics of Semiconductor Devices. Wiley-Interscience, New York, 43, 245, 410-414.

[7] Juang, F.S. and Su, Y.K. (1989) *Solid-State Electronics*, **32**, 661-664. https://doi.org/10.1016/0038-1101(89)90145-7

[8] Malacky, L., Kordos, P. and Novak, J. (1990) *Solid-State Electronics*, **33**, 273-278. https://doi.org/10.1016/0038-1101(90)90166-C

[9] Sarpatwari, K. (2009) Toward Understanding the Electrical Properties of Metal/Semiconductor Schottky Contacts: The Effects of Barrier Inhomogeneities and Geometry in Bulk and Nanoscale Structures. PhD Thesis, The Pennsylvania State

University, The Graduate School, State College.

[10] Mikhelashvili, V.B., Eisenstein, G., Valery, G. and Fainleib, S. (1999) *Journal of Applied Physics*, **85**, 6873-6883. https://doi.org/10.1063/1.370206

[11] Norde, H. (1979) *Journal of Applied Physics*, **50**, 5052-5053. https://doi.org/10.1063/1.325607

[12] Cibils, R.M. and Buitrago, R.H. (1985) *Journal of Applied Physics*, **58**, 1075-1077. https://doi.org/10.1063/1.336222

[13] Sato, K. and Yasumura, Y. (1985) *Journal of Applied Physics*, **58**, 3655-3657. https://doi.org/10.1063/1.335750

[14] Cheung, S.K. and Cheung, N.W. (1986) *Applied Physics Letters*, **49**, 85-87. https://doi.org/10.1063/1.97359

[15] Bohlin, K.E. (1986) *Journal of Applied Physics*, **60**, 1223-1224. https://doi.org/10.1063/1.337372

[16] Chin, V.W.L., Storey, J.W.V. and Green, M. (1989) *Solid-State Electronics*, **32**, 475-478. https://doi.org/10.1016/0038-1101(89)90029-4

[17] Osvald, J. and Dobrocka, E. (1996) *Semiconductor Science and Technology*, **11**, 1198. https://doi.org/10.1088/0268-1242/11/8/014

[18] Mikhelashvili, V.B., Eisenstein, G. and Uzdin, R. (2001) *Solid-State Electronics*, **45**, 143-148. https://doi.org/10.1016/S0038-1101(00)00227-6

[19] Safak, H., Sahin, M. and Yüksel, O.F. (2002) *Solid-State-Electronics*, **46**, 49-52. https://doi.org/10.1016/S0038-1101(01)00273-8

[20] Bouzidi, K., Chegear, M. and Aillerie, M. (2012) *Energy Procedia*, **18**, 1601-1610. https://doi.org/10.1016/j.egypro.2012.06.001

[21] Karboyan, S., Tartarin, J.-G. and Lambert, B. (2013) Analysis of Barrier Inhomogeneities in AlGaN/GaN HEMTs' Schottky Diodes by I-V-T Measurements. EuMC, Oct. 2013, Nuremberg, Germany. 4 p. hal-01343345.

[22] Jyotti, I., Yang, H.-D., Choi, C.J., *et al.* (2013) *Materials Transactions*, **54**, 1655-1660. https://doi.org/10.2320/matertrans.M2013015

[23] Liu, Y., Tang, W.M. and Lai, P.T. (2016) *Physica Status Solidi* (*a*), **213**, 2764-2768. https://doi.org/10.1002/pssa.201600110

[24] Mayimele, M.A., Auret, F.D., Janse van Rensburg, J.P. and Diale, M. (2016) Analysis of Temperature-Dependent Current-Voltage Characteristics and Extraction of Series Resistance in Pd/ZnO Schottky Barrier Diodes. https://doi.org/10.1016/j.physb.2015.07.034

[25] Ghizlane, T., Hassan, O., Abdelkader, B. and Omar, B. (2018) *Periodicals of Engineering and Natural Sciences*, **6**, 331-337. https://doi.org/10.21533/pen.v6i2.535

[26] Sadoon, A. and Kemerchou, I. (2020) *International Journal of Energetica*, **5**, 31-37. https://doi.org/10.47238/ijeca.v5i1.120

[27] Wong, C.P.Y., Troadec, C., Wee, A.T.S. and Goh, K.E.J. (2020) *Physical Review Applied*, **14**, Article ID: 054027. https://doi.org/10.1103/PhysRevApplied.14.054027

[28] Lee, J.I., Brini, J. and Dimitriadis, C.A. (1998) *Electronics Letters*, **34**, 1268-1269. https://doi.org/10.1049/el:19980831

[29] NREL (2006) Measurements & Characterization: Electro-Optical Characterization. National Renewable Energy Laboratory, National Center for Photovoltaics, Middlewest Research Institute, Battele, Golden, NREL/BR-520-40121.

[30] Devi, V.L., Jyothi, I., Reddy, V.R. and Choi, C.-J. (2012) *The Open Applied Physics Journal*, **5**, 1-9. https://doi.org/10.2174/1874183501205010001

[31] Broom, R.F., Meier, H.P. and Walter, W. (1986) *Journal of Applied Physics*, **60**, 1832-1833. https://doi.org/10.1063/1.337226

[32] Cova, P. and Singh, A. (1990) *Solid-State Electronics*, **33**, 11-19. https://doi.org/10.1016/0038-1101(90)90003-W

[33] Chin, V.W.L., Green, M. and Storey, J.W.V. (1990) *Solid-State Electronics*, **33**, 299-308. https://doi.org/10.1016/0038-1101(90)90170-J

[34] Clifford, J.P., Johnson, K.W., Levina, L. and Sargent, E.H. (2007) *Applied Physics Letters*, **91**, Article ID: 253113. https://doi.org/10.1063/1.2823582

[35] Singh, A., Cova, P. and Masut, R.A. (2011) Parameter Extraction from Reverse I-V and C-V Characteristics in an Epitaxial p-InP/Au Schottky Diode. Volume 318, Cambridge University Press, MRS Online Library (OPL), Cambridge. https://doi.org/10.1557/PROC-318-135

[36] Kudryk, Y.Y., Shynkarenko, V.V., Kudryk, R.Y., *et al.* (2014) *Semiconductor Physics, Quantum Electronics & Optoelectronics*, **17**, 398-402. https://doi.org/10.15407/spqeo17.04.398

[37] An, Y., Behnam, A., Pop, E. and Ural, A. (2015) *Journal of Applied Physics*, **118**, Article ID: 114307. https://doi.org/10.1063/1.4931142

[38] Ali, M.H., Rabhi, A., Haddad, S. and El Hajjaji, A. (2017) *Journal of Electronic Materials*, **46**, 6535-6543. https://www.researchgate.net/publication/318690056

[39] Lakehal, B. and Dendouga, A. (2018) *Journal of Nano- and Electronic Physics*, **10**, Article ID: 06046. https://doi.org/10.21272/jnep.10(6).06046

[40] Jang, J.T., Min, J., Kim, D.M., *et al.* (2019) SPICE Compact Model of IGZO Memristor Based on Non-Quasi-Statistically Updated Schottky Barrier Height. *Proceedings of the* 19*th IEEE International Conference on Nanotechnology*, Macau, 22-26 July 2019, 562-565. https://doi.org/10.1109/NANO46743.2019.8993957

[41] Garoudja, E., Falali, W., Oussalah, S., Sengouga, N. and Henini, M. (2020) *Journal of Semiconductors*, **41**, Article ID: 102401. https://doi.org/10.1088/1674-4926/41/10/102401

[42] Liu, X., Zhang, Y., Jin, Z., *et al.* (2021) *Electronics*, **10**, 1540. https://doi.org/10.3390/electronics10131540

[43] Bashahu, M. and Habyarimana, A. (1995) *Renewable Energy*, **6**, 129-138. https://doi.org/10.1016/0960-1481(94)E0021-V

[44] Bashahu, M. and Nkundabakura, P. (2007) *Solar Energy*, **81**, 856-863. https://doi.org/10.1016/j.solener.2006.11.002

[45] Cotfas, D.T., Cotfas, P.A. and Kaplanis, S. (2013) *Renewable and Sustainable Energy Reviews*, **28**, 588-596. https://doi.org/10.1016/j.rser.2013.08.017

[46] Cotfas, D.T., Cotfas, P.A. and Kaplanis, S. (2016) *Renewable and Sustainable Energy Reviews*, **61**, 213-221. https://doi.org/10.1016/j.rser.2016.03.051

[47] Ferhat-Hamida, A., Ouennoughi, Z., Hoffmann, A. and Weiss, R. (2002) *Solid-State Electronics*, **46**, 615-619. https://doi.org/10.1016/S0038-1101(01)00337-9

[48] Araujo, G.L., Sanchez, E. and Marti, M. (1982) *Solar Cells*, **5**, 199-204. https://doi.org/10.1016/0379-6787(82)90027-8

[49] Lee, H.-Y. and Lee, C.-T. (2003) *Solid-State Electronics*, **47**, 831-834. https://doi.org/10.1016/S0038-1101(02)00372-6

[50] Liang, G., Cui, T. and Varahramyan, K. (2003) *Solid-State Electronics*, **47**, 691-694. https://doi.org/10.1016/S0038-1101(02)00324-6

[51] Zhu, S., Detavernier, C., Li, B.-Z., *et al.* (2000) *Solid-State Electronics*, **44**, 1807-1818.

https://doi.org/10.1016/S0038-1101(00)00127-1

[52] Donoval, D., De Sousa Pires, J., Tove, P.A. and Harman, R. (1989) *Solid-State Electronics*, **32**, 961-964. https://doi.org/10.1016/0038-1101(89)90156-1

[53] Aniltürk, Ö.S. and Turan, R. (2000) *Solid-State Electronics*, **44**, 41-48. https://doi.org/10.1016/S0038-1101(99)00204-X

[54] Pristavu, G., Brezeanu, G., Pribeanu, A., *et al.* (2017) *Materials Science Forum*, **897**, 606-609. https://doi.org/10.4028/www.scientific.net/MSF.897.606

[55] Levinshtein, M., *et al.* (1996) Appendices: 1. Basic Physical Constants. In: Levinshtein, M., Rumyantsev, S. and Shur, M., Eds., *Handbook Series on Semiconductor Parameters*, Volume 1, World Scientific Publishing Co. Pte. Ltd., Singapore, 214. https://doi.org/10.1142/9789812832078_bmatter